A blind steganography approach for hiding privacy details in images of digital imaging and communications in medicine using QR code

Mahmoud Rashad[1], Ahmed Elhadad[2,3], Kamal El-Saady[1]
[1]Department of Mathematics and Computer Science, Faculty of Science, South Valley University, Qena, Egypt
[2]Department of Computer Science, Faculty of Computer and Information Sciences, South Valley University, Qena, Egypt
[3]Department of Computer Science and Information, Faculty of Science and Art, Jouf University, Al Qurayyat, Kingdom of Saudi Arabia

Article Info

Article history:

Received May 19, 2021
Revised Mar 17, 2022
Accepted Mar 30, 2022

Keywords:

Data hiding
DICOM
Discrete cosine transform
Medical images
QR code

ABSTRACT

This study aims to hide patient's privacy details of digital imaging and communications in medicine (DICOM) files using the quick response (QR) code images with the same size using steganographic technique. The proposed method is based on the properties of the discrete cosine transform (DCT) of the DICOM images to embed a QR code image. The proposed method includes two parts: data embedding and extraction process. Moreover, the stego DICOM image could be blindly used to produce the embedded QR code image without the existence of the original DICOM image. The performances of proposed method were evaluated using the metrics of the peak signal to noise ratio (PSNR), the structural similarity index (SSIM), the universal quality index (UQI), the correlation coefficient (R) and the bit error rate (BER) values. The experimental results scored a high PSNR after the embedding process by embedding a QR code image into the DICOM image with the same size.

Corresponding Author:

Ahmed Elhadad
Department of Computer Science, Faculty of Computer and Information Sciences, South Valley University
Qena, Egypt
Email: ahmed.elhadad@sci.svu.edu.eg

1. INTRODUCTION

Digital imaging and communications in medicine (DICOM) is the standard medical imaging data format, which is most used for the exchanging, management and viewing of medical images, such as computerized tomography (CT) scans, magnetic resonance imaging tests (MRIs), and ultrasound images [1]. The DICOM format was developed and copyrighted by the National Electrical Manufacturers Association (NEMA) [2], [3]. It has been broadly espoused by hospitals and is making inroads into smaller applications like labs and dentists' and doctors' offices. The DICOM frequently parsed and enables the integration between different devices and platforms which using the picture archiving and communication system (PACS) [4]–[8].

The medical information of patients must be protected from unauthorized access. Generally, the medical information security refers to the rules of security policies that strict ethics rights and privacy of the patient and must be concerned by entities. There are many widely used standards and tools for protecting personal medical information such as the ISO27799 (security management in health using ISO/IEC/27799) [9], cryptography and steganography techniques [10]–[13]. The ISO27799 is a standard which provides the security management guidelines for health organizations to protect medical information. Cryptography is a data protection using encryption provider which converts the medical information into unintelligible text using secure key. Steganography can be defined as the use of a host (container) data to hide or embed a piece of information that is hidden directly in media content, in such a way that it is imperceptible to a human observer but can be detected/extracted easily with a computer [14], [15].

The quick response code is always abbreviated to QR code which is a barcode that is readable by an imaging device such as a camera and smartphones. The QR code system was originally invented and designed in 1994 by the Japanese Company Denso Wave and it was registered as a trademark of the same company [16], [17]. Simply, the QR code is a matrix code of two-dimensional barcodes and consists of black squares arranged in a square grid on a white background. Unlike the one-dimensional barcodes that were designed to be scanned by a narrow beam of light, the QR code is scanned by a digital image sensor and then digitally analyzed by a programmed processor. The QR code includes three main distinct squares at the corners to set up the image size normalization, orientation, and angle of viewing. Moreover, the small dots throughout the QR code are then converted to binary numbers and validated with the Reed–Solomon error-correcting algorithm [18] which are encoded as bytes of 8 bits. In practice, QR codes often contain data for a locator, identifier, or tracker that points to a standard URL for a website or application. A QR code uses four standardized encoding modes (numeric-Max. 7,089 characters, alphanumeric- Max. 4,296 characters, byte/binary-Max. 2,953 characters, and kanji-Max. 1,817 characters) to store the amount of data efficiently; extensions may also be used [18].

The rest of this paper is organized as follows: section 2 presents the used materials and methods. The proposed method is illustrated in detail in section 3. Section 4 shows the experimental results and discussions. Finally, the study and the main contributions are concluded in section 5.

2. MATERIALS AND METHODS

2.1. The cancer imaging archive (TCIA) COVID-19 dataset

This study aims to hide patient's privacy details of DICOM files using the QR code images therefore, TCIA COVID-19 dataset is used [19]–[22]. TCIA COVID-19 dataset is a chest radiology imaging with CT imaging studies, a set of clinical data and key radiology findings for patients representing a rural COVID-19 positive population in the state of Arkansas. These data are cross-linked to severe acute respiratory syndrome coronavirus 2 (SARS-CoV-2) complimentary DNA (cDNA) sequence data extracted from clinical isolates from the same population, uploaded to the GenBank repository. This collection dataset includes 105 patient's data with 31,935 total number of images, 256 number of studies, 461 number of series and 19.0 GB images size. The TCIA COVID-19 dataset provides three study modality computed radiography (CR): (26 images (0.1%), 19 patients), direct digital capture (DX): (236 images (0.7%), 100 patients) and computed tomography (CT): (31673 images (99.2%), 23 patients). In addition, the dataset provides different images size between 350×552 to 3366×3006 using DICOM standard format. Figure 1 shows image samples description of the TCIA COVID-19 dataset.

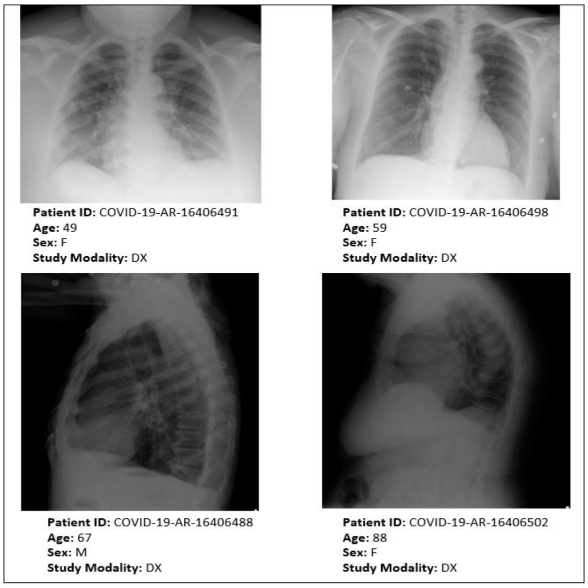

Figure 1. DICOM images samples of TCIA COVID-19 dataset

2.2. The QR code

In this paper, the QR Code generator is based on the zebra crossing (ZXing) library [23]–[25]. The QR code generator is a software that creates data into a QR code image using the format information of two things: the error correction level and the mask pattern used for the symbol. The mask patterns are specified on a grid that is repeated as necessary to cover the whole symbol and protected from errors with a Bose-Chaudhuri–Hocquenghem (BCH) code and a double of complete copies are included in each QR pattern. Hence, ZXing is an open-source library project implemented in Java, with ports to other languages which supports generating and decoding of multi-format 1D/2D barcode image processing such as QR code and data matrix within images and all files can be imported on the fly from a maven repository or can be downloaded via a command. Figure 2 shows the generated four QR codes of various size which are used as an embedded image within the DICOM files.

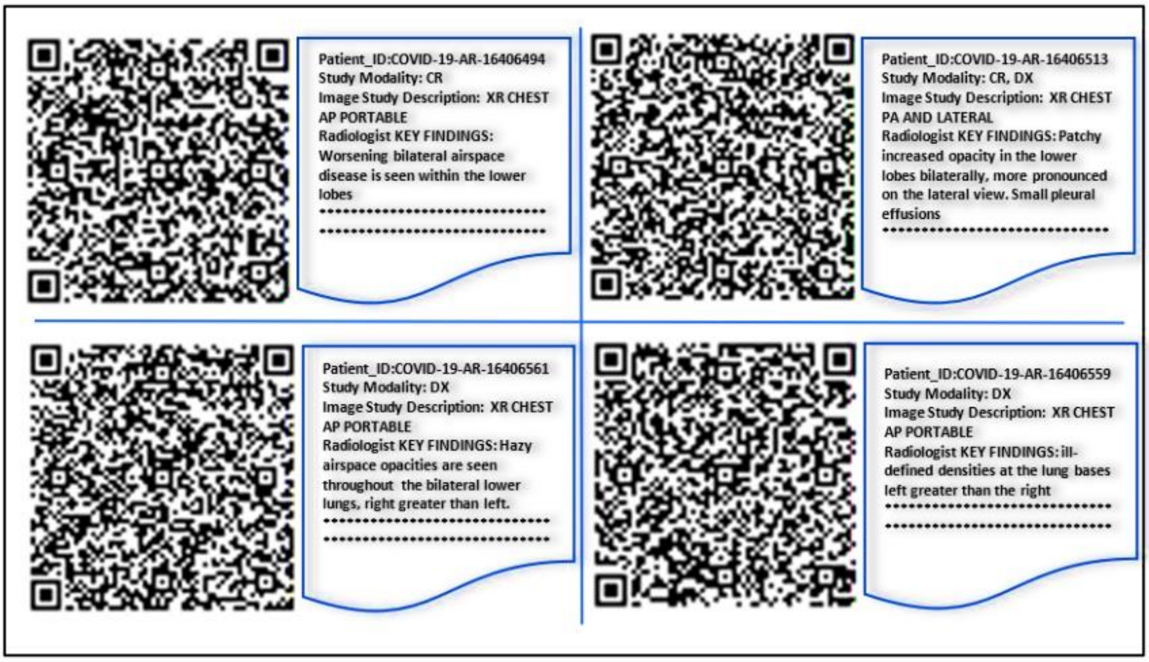

Figure 2. QR code examples of various size and corresponding decoded text

3. THE PROPOSED METHOD

Figure 3 shows a high-level overall view of the main parts of the proposed method to embed patient information into the DICOM image. The main idea of this method is to generate a new image (stego) whose pixels are combination of two images with the same size where one of them is used as cover and the other is the secret message (Msg). The generated stego image should be similar to the cove image with little distortion as possible. Then this stego image could be blindly used to produce the embedded massage without the existence of the original image. The proposed method includes two parts: data embedding and extraction process.

3.1. Data embedding process

In this process, the data embedding process mainly focuses on embedding the QR code image into the DICOM image. The proposed method collects patient information from the DICOM file and the corresponding clinical data such as patient ID, image study description, study modality and radiologist key findings. Next, the proposed method generates a QR code image using the collected patient data then it resizes the QR code image to be compatible with the cover DICOM image. As a preprocessing stage, both the QR code image and the cover DICOM image are normalized and adjusted to get float pixel values whose pixels have float values that belong to the interval [0, 1] instead of the integer range and to avoid an overflow in the embedded stego coefficients of saturated pixel values (0 or 1) using a small value (α) respectively.

$$Normalization(Img) = \frac{Img - Min(Img)}{\max(Img) - Min(Img)} \quad (1)$$

$$Adjustment(Img) = \begin{cases} 1-\ \alpha, & Img \geq 1 \\ \alpha, & Img = 0 \end{cases} \quad (2)$$

After normalization and adjustment are done, in preprocessing stage, the resultant cover and QR code images are divided into small parts of 4×4 matrices called micro-blocks (MB). Then the embedding process stage is ready to start.

In the embedding process, the main aim of this step is to embed the normalized MB of the QR code image into the corresponding normalized MB of the cover DICOM image to construct integrated stego DICOM image. Thus, 2-D discrete cosine transform (DCT) is applied on the cover's MBs.

$$DCT\ coefficients = T\ \times MB_{Cover} \times T' \quad (3)$$

$$T = \begin{bmatrix} \frac{1}{\sqrt{4}} & \frac{1}{\sqrt{4}} & \frac{1}{\sqrt{4}} & \frac{1}{\sqrt{4}} \\ \sqrt{\frac{2}{4}}Cos(\frac{\pi}{8}) & \sqrt{\frac{2}{4}}Cos(\frac{3\pi}{8}) & \sqrt{\frac{2}{4}}Cos(\frac{3\pi}{8}) & \sqrt{\frac{2}{4}}Cos(\frac{3\pi}{8}) \\ \sqrt{\frac{2}{4}}Cos(\frac{3\pi}{8}) & \sqrt{\frac{2}{4}}Cos(\frac{3\pi}{8}) & \sqrt{\frac{2}{4}}Cos(\frac{3\pi}{8}) & \sqrt{\frac{2}{4}}Cos(\frac{3\pi}{8}) \\ \sqrt{\frac{2}{4}}Cos(\frac{3\pi}{8}) & \sqrt{\frac{2}{4}}Cos(\frac{3\pi}{8}) & \sqrt{\frac{2}{4}}Cos(\frac{3\pi}{8}) & \sqrt{\frac{2}{4}}Cos(\frac{3\pi}{8}) \end{bmatrix}$$

The resultant matrix consists of 4×4 coefficients; one approximation and fifteen details coefficients. Next, the embedding process is carried out on the cover DCT coefficients by replacing these coefficients with the corresponding normalized QR code image's MB pixel values using (4).

$$Stego\ coefficient = \ sign(DCT\ coefficient_{Cover}) \left[\frac{2}{\beta}(MB_{QR\ code} + i), \frac{2i}{\beta} \leq |DCT\ coefficient_{Cover}| \leq \frac{2(i+1)}{\beta}\right] \quad (4)$$

$$\forall\ i = 0,1,2, \ldots\ , \beta - 1$$

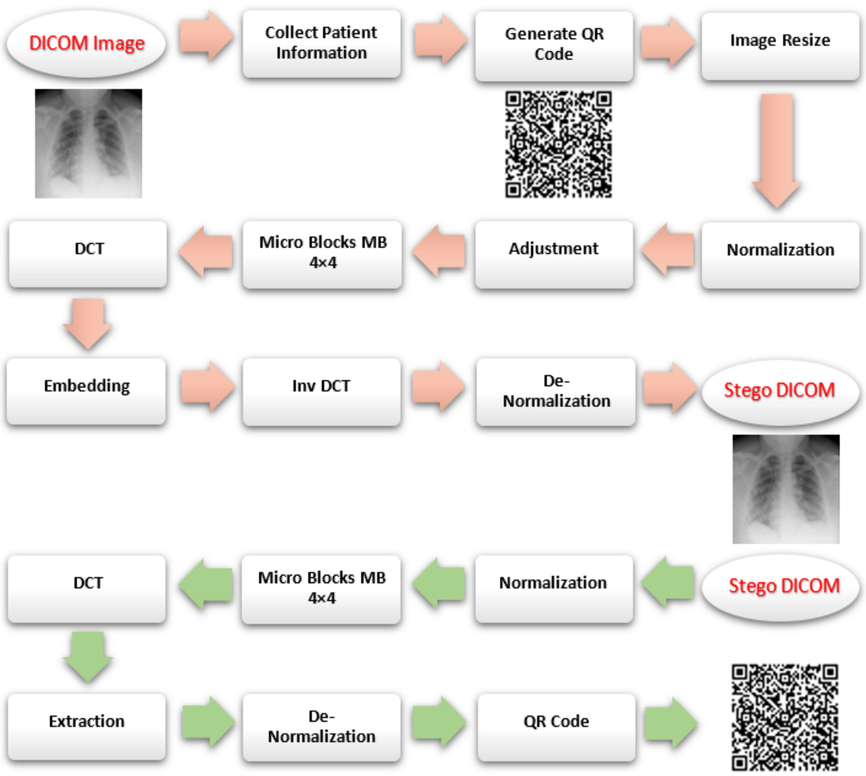

Figure 3. A high-level overall view of the proposed method to embed patient information into DICOM image

The absolute values of the DCT coefficients lies in the interval [0, 2] where the range is actually determined by the minimum and maximum for each coefficient value Thus, β is an additional parameter that will be used to divide the range [0, 2] of the absolute value of the cover DCT coefficients. To improve stego image quality against noise, the approximation coefficient value of the cover image is kept without modification during the embedding process for each MB. After the embedding process is done, the stego DICOM image is obtained by applying the inverse DCT (Inv. DCT) then denormalization is applied to convert the pixel values back to their original domain using (5).

$$MB_{Stego} = T' \times DCT_{Stego}\ coefficients\ \times T \tag{5}$$

Finally, the resultant stego image is saved as a medical image in DICOM format.

3.2. Data extraction process

The steps of extraction process are exactly the inverse of those followed during the embedding phases. Therefore, these process starts by read the stego DICOM image then apply the normalization to convert the pixel values to [0, 1] domain. Next, the normalized stego DICOM image is divided into 4×4 MB and compute the DCT decomposition using (6).

$$DCT\ coefficients = T\ \times MB_{Stego} \times T' \tag{6}$$

After that, the extraction stage is applied on the stego DCT coefficients:

$$MB_{Rec-QR\ code} = \frac{\beta}{2}\left(DCT\ coefficient_{Stego} - \frac{2i}{\beta}\right),\ \frac{2i}{\beta} \leq |DCT\ coefficient_{Stego}| \leq \frac{2(i+1)}{\beta} \tag{7}$$

$$\forall\ i = 0,1,2, \dots ,\beta - 1$$

where β is the same integer number is used in the embedding stage. In addition, to correctly reconstruct the first element in $MB_{Rec\text{-}QR\ code}$, the mean value of three neighbors is calculated and replaced on it. Finally, the resultant *Rec-QR code* is denormalized to set the pixel values back to their original domain which is similar to the original QR code image.

4. RESULTS AND DISCUSSION

This section discusses and analysis the results of the proposed method using the TCIA COVID-19 dataset, which was obtained from [19]–[22] that includes 105 patient’s data with 31,935 total number of images, 256 number of studies, 461 number of series and 19.0 GB images size. The simulation was implemented using MATLAB version: 9.3.0.713579 (R2017b) with the image processing toolbox and includes read DICOM image function for image importing and conversion.

Figure 4 shows the DICOM image, QR code image, stego DICOM and reconstructed QR code image samples from two patients’ TCIA COVID-19 images of the proposed method. Figures 4(a) to (d) illustrate the cover DICOM and the QR code images respectively however Figures 4(e) and 4(f) show the resultant stego DICOM image after embedding the QR code image into the cover DICOM image. Moreover, Figures 4(g) and 4(h) show the reconstructed QR code image after applying the extraction process from stego DICOM images by an authorized person. The simple visual inspection of the results shows a very high quality of the stego DICOM images while providing a scannable visual quality for the retrieved QR code image.

The performances of proposed method were evaluated using the peak signal to noise ratio (PSNR), the structural similarity index (SSIM), the universal quality index (UQI), and the correlation coefficient (R) values, whose details were explained:

$$PSNR = 10 \log_{10}\left(\frac{peakval^2}{MSE}\right) \tag{8}$$

$$MSE = \frac{1}{MN}\sum_{i=0}^{M-1}\sum_{j=0}^{N-1}\left(f(x_i, y_j) - g(x_i, y_j)\right)^2$$

where *f(x, y)* and *g(x, y)* defined the cover and stego patients’ images. M and N are the height and width of the images. The peakval is the range of the image data type (e.g., for uint16 image it is 65535). Figure 5 shows the resultant mean of PSNR values to compare between cover and stego DICOM images in decibel (dB). The mean PSNR values ranged between 63.47 dB and 81.97 dB for various values of β. The minimum and maximum value of the mean PSNR are 50.41 dB and 95.33 dB respectively. Generally, PSNR higher values refers that the invisibility of higher quality.

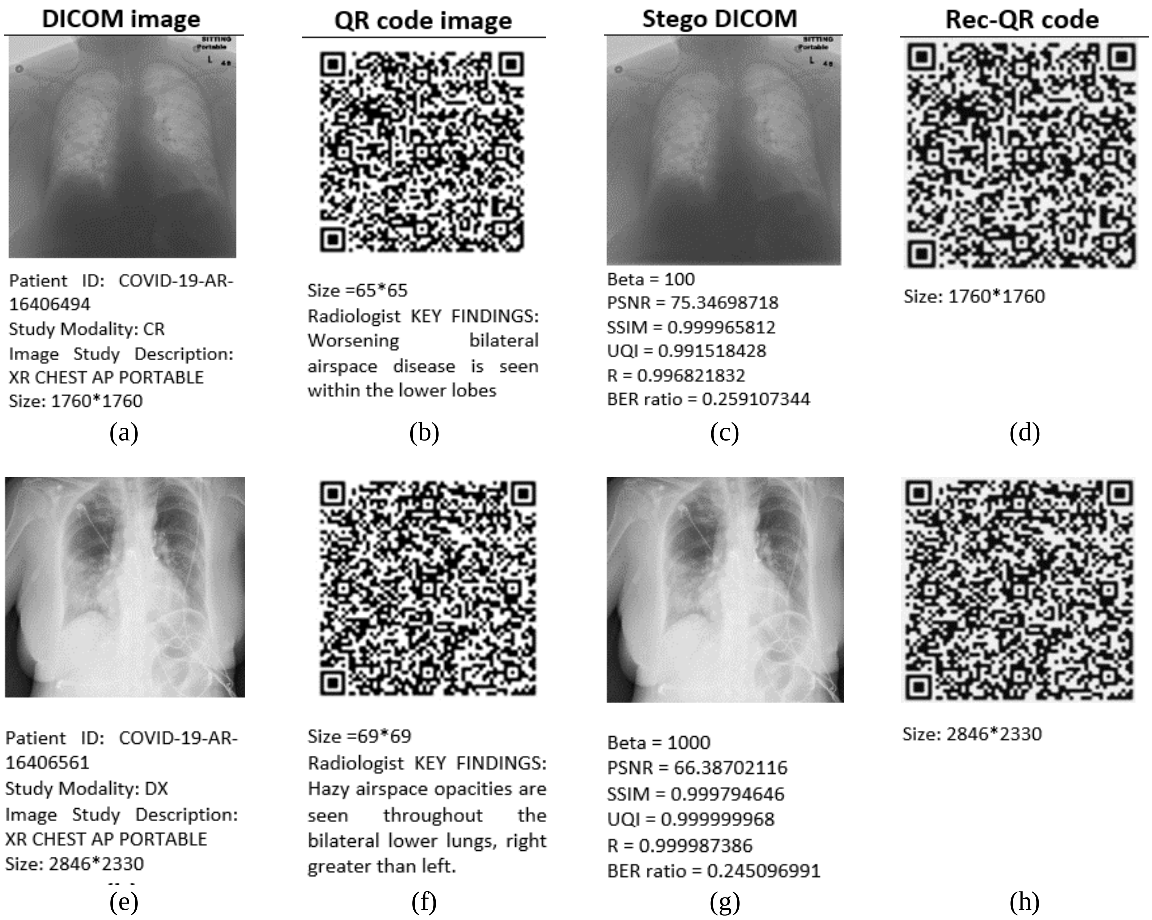

Figure 4. DICOM images samples of COVID-19-AR-16406494 and COVID-19-AR-16406561 and the results DICOM images of the proposed data hiding method: (a) to (d) illustrate the cover DICOM and the QR code images respectively, (e) and (f) the resultant stego DICOM image after embedding the QR code image into the cover DICOM image, (g) and (h) the reconstructed QR code image

The PSNR is approach to human observation of invisibility quality with the human visual system (HVS). On the other hand, the structural similarity (SSIM) index is a perceptual metric that quantifies image quality degradation as perceived change in structural information [26], [27]. In addition, the universal image quality index (UQI) proposed by Wang and Bovik evaluates the loss of correlation, luminance distortion, and contrast distortion [28], [29]. Therefore, the performances of SSIM and UQI are better than the MSE and PSNR. Equations (9) and (10) illustrate the SSIM and the UQI in details:

$$SSIM(x,y) = \frac{(2\mu_x\mu_y+c_1)(2\sigma_{xy}+c_2)}{(\mu_x^2+\mu_y^2+c_1)(\sigma_x^2+\sigma_y^2+c_2)} \tag{9}$$

$$UQI(x,y) = \frac{(4\mu_x\mu_y 2\sigma_{xy})}{(\mu_x^2+\mu_y^2)(\sigma_x^2+\sigma_y^2)} \tag{10}$$

where μ_x and μ_y are the local means, σ^2_x and σ^2_y are the variance of x and y. σ_{xy} is the cross-covariance for images x, y. c_1 and c_2 are variables to stabilize the division with weak denominator. The correlation coefficient (R) is widely used in statistical analysis to compare two images in image processing purposes [30]–[33]. Equation (11) describes R in detail:

$$R = \frac{\sum_X \sum_Y (f_{XY} - \bar{f}) - (g_{XY} - \bar{g})}{\sqrt{(\sum_X \sum_Y (f_{XY} - \bar{f})^2)(\sum_X \sum_Y (g_{XY} - \bar{g})^2)}} \quad (11)$$

where $\bar{f}$ and $\bar{g}$ are the mean of cover and stego patients' images pixels. Figure 6 shows the mean of the obtained SSIM to compare between the cover and resultant stego images. The minimum and maximum mean values of the SSIM confined between 0.979 and 1 while the overall mean SSIM values between 0.9964 and 1. Figure 7 and Figure 8 illustrate the obtained results of the mean UQI and the mean R respectively. The minimum and maximum values of the mean UQI are ranged between 0.48 and 1 while the minimum and maximum values of the mean R are recorded between 0.93 and 1. From the obtained PSNR, SSIM, UQI and R results, the value of the parameter β always effects on the resultant quality of the stego patients' image where the high β values produce high quality stego DICOM image.

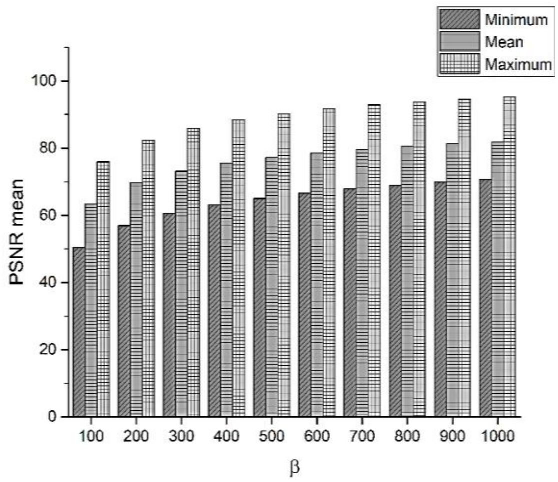

Figure 5. The mean of resultant PSNR for stego and cover patients' DICOM images

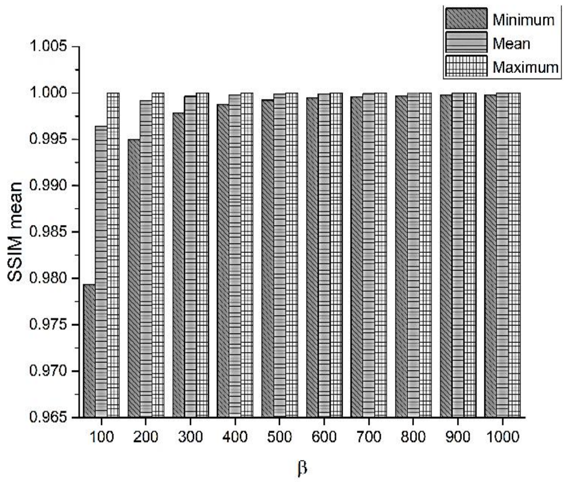

Figure 6. The mean of resultant SSIM for stego and cover patients' DICOM images

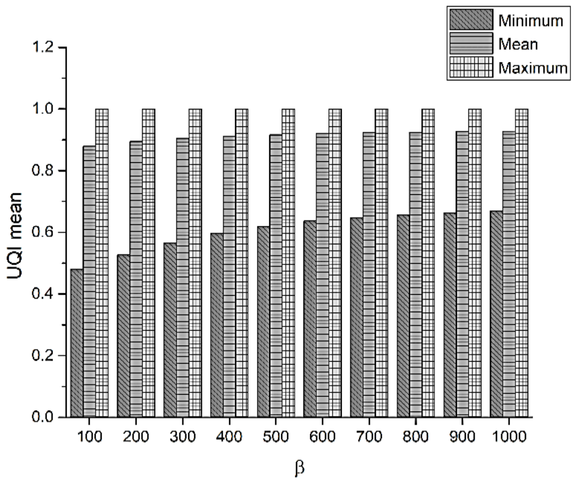

Figure 7. The mean of resultant UQI for stego and cover patients' DICOM images

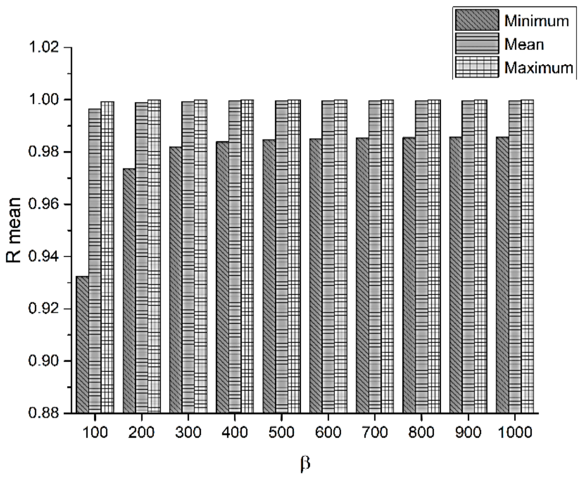

Figure 8. The mean of resultant R for stego and cover patients' DICOM images

Finally, the bit error rate (BER), returned as a scalar which is the number of bit errors to the total number of bits used in the binary representation. Figure 9 shows the mean BER between the cover and stego patients' DICOM images for various values of β. The mean BER values ranged between 0.1632 and 0.2820. The minimum and maximum values of the mean BER are 0.03 and 0.34 respectively.

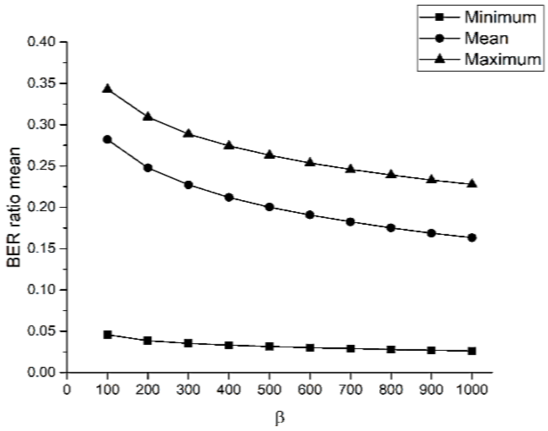

Figure 9. The mean of resultant BER for stego and cover patients' DICOM images

5. CONCLUSION

Most DICOM objects contain images and associated demographic and medical information about the patient, which need to be kept confidential. Cryptography and steganography are generally used to ensure medical information of patients' security. Therefore, this study aims to hide patient's privacy details of DICOM files using the QR code images. Different sized 31,935 images of 105 patients were used as cover and embedded QR code images. The main idea of this method is to generate a new image (stego) whose pixels are combination of two images with the same size where one of them is used as cover and the other is the secret message (Msg). The generated stego image should be similar to the cove image with little distortion as possible. Then this stego image could be blindly used to produce the embedded massage without the existence of the original image. The performances of proposed method were evaluated using PSNR, SSIM, UQI, R and BER metrics. The mean PSNR values ranged between 63.47 dB and 81.97 dB.

REFERENCES

[1] E. Seeram, "Medical imaging informatics: an overview," in *Digital Radiography*, Springer Singapore, 2019, pp. 165–183.
[2] DICOM, "DICOM PS3.3 2019d-information object definitions," dicomstandard.org, Accessed: Jan. 20, 2021. [Online]. Available: http://dicom.nema.org/medical/dicom/current/output/chtml/part03/sect_C.7.6.3.html
[3] D. E. Best, S. C. Horii, W. C. Bennett, and C. R. Parisot, "Update of the ACR-NEMA digital imaging and communications in medicine standard," in *Medical Imaging VI: PACS Design and Evaluation*, 1992, vol. 1654, pp. 356–361, doi: 10.1117/12.60322.
[4] Y. H. Su and C.-C. Jay Kuo, "Fast and robust camera's auto exposure control using convex or concave model," in *2015 IEEE International Conference on Consumer Electronics (ICCE)*, Jan. 2015, pp. 13–14, doi: 10.1109/ICCE.2015.7066300.
[5] Y. Su and C. C. J. Kuo, "On extended long short-term memory and dependent bidirectional recurrent neural network," *Neurocomputing*, vol. 356, pp. 151–161, Sep. 2019, doi: 10.1016/j.neucom.2019.04.044.
[6] Y. Su, Y. Huang, and C.-C. J. Kuo, "Efficient text classification using tree-structured multi-linear principal component analysis," in *24th International Conference on Pattern Recognition (ICPR)*, Aug. 2018, pp. 585–590, doi: 10.1109/ICPR.2018.8545832.
[7] Y. Su, J. Y. Lin, and C.-C. J. Kuo, "A model-based approach to camera's auto exposure control," *Journal of Visual Communication and Image Representation*, vol. 36, pp. 122–129, Apr. 2016, doi: 10.1016/j.jvcir.2016.01.011.
[8] Y. Su, R. Lin, and C.-C. Jay Kuo, "Tree-structured multi-stage principal component analysis (TMPCA): theory and applications," *Expert Systems with Applications*, vol. 118, pp. 355–364, Mar. 2019, doi: 10.1016/j.eswa.2018.10.020.
[9] ISO, "27799-health informatics-information security management in health using ISO," ISO, Accessed: Mar. 14, 2019. [Online]. Available: https://www.iso.org/obp/ui/#iso:std:iso:27799:ed-2:v1:en
[10] A. Elhadad, A. Ghareeb, and S. Abbas, "A blind and high-capacity data hiding of DICOM medical images based on fuzzification concepts," *Alexandria Engineering Journal*, vol. 60, no. 2, pp. 2471–2482, Apr. 2021, doi: 10.1016/j.aej.2020.12.050.
[11] A. Elhadad, S. Hamad, A. Khalifa, and H. Abulkasim, "A steganography approach for hiding privacy in video surveillance systems," in *Digital Media Steganography*, Elsevier, 2020, pp. 165–187.
[12] O. H. Khalil, A. Elhadad, and A. Ghareeb, "A blind proposed 3D mesh watermarking technique for copyright protection," *The Imaging Science Journal*, vol. 68, no. 2, pp. 90–99, Feb. 2020, doi: 10.1080/13682199.2020.1740431.
[13] A. Elhadad, "Data sharing using proxy re-encryption based on DNA computing," *Soft Computing*, vol. 24, no. 3, pp. 2101–2108, Feb. 2020, doi: 10.1007/s00500-019-04041-z.
[14] G. J. Simmons, "The prisoners' problem and the subliminal channel," in *Advances in Cryptology*, MA: Springer US, 1984, pp. 51–67.
[15] A. Elhadad, S. Hamad, A. Khalifa, and A. Ghareeb, "High capacity information hiding for privacy protection in digital video files," *Neural Computing and Applications*, vol. 28, no. 1, pp. 91–95, Dec. 2017, doi: 10.1007/s00521-016-2323-7.
[16] K. Peng, H. Sanabria, D. Wu, and C. Zhu, "Security overview of QR codes," *Student project in the MIT course*, vol. 6, pp. 1–20, 2014.
[17] S. Tiwari, "An introduction to QR code technology," in *2016 International Conference on Information Technology (ICIT)*, Dec. 2016, pp. 39–44, doi: 10.1109/ICIT.2016.021.
[18] Denso Wave Inc. "QR code essentials." Denso Wave, vol. 900, 2011.

[19] S. Desai *et al.*, “Data from chest imaging with clinical and genomic correlates representing a rural covid-19 positive population,” *The Cancer Imaging Archive*, 2020.
[20] S. Desai *et al.*, “Chest imaging representing a COVID-19 positive rural U.S. population,” *Scientific Data*, vol. 7, no. 1, Dec. 2020, doi: 10.1038/s41597-020-00741-6.
[21] P. Jenjaroenpun *et al.*, “Two SARS-CoV-2 genome sequences of isolates from rural U.S. patients harboring the D614G mutation, obtained using nanopore sequencing,” *Microbiology Resource Announcements*, vol. 10, no. 1, 2021, doi: 10.1128/MRA.01109-20.
[22] K. Clark *et al.*, “The cancer imaging archive (TCIA): maintaining and operating a public information repository,” *Journal of Digital Imaging*, vol. 26, no. 6, pp. 1045–1057, Dec. 2013, doi: 10.1007/s10278-013-9622-7.
[23] J. Richter, “QR code generator 1.1 based on zxing,” 2020, Accessed: Jan. 18, 2021. [Online]. Available: https://www.mathworks.com/matlabcentral/fileexchange/49808-qr-code-generator-1-1-based-on-zxing
[24] T. Dean and C. Dunn, “Quick layered response (QLR) codes.” Department of Electrical Engineering, Stanford University, Tech. Rep., 2012.
[25] M. B. Hoy, “An introduction to QR codes: linking libraries and mobile patrons,” *Medical Reference Services Quarterly*, vol. 30, no. 3, pp. 295–300, Jul. 2011, doi: 10.1080/02763869.2011.590423.
[26] M.-J. Chen and A. C. Bovik, “Fast structural similarity index algorithm,” *Journal of Real-Time Image Processing*, vol. 6, no. 4, pp. 281–287, Dec. 2011, doi: 10.1007/s11554-010-0170-9.
[27] A. Hore and D. Ziou, “Image quality metrics: PSNR vs. SSIM,” in *2010 20th International Conference on Pattern Recognition*, Aug. 2010, pp. 2366–2369, doi: 10.1109/ICPR.2010.579.
[28] A. Toet and M. A. Hogervorst, “Performance comparison of different gray-level image fusion schemes through a universal image quality index,” in *Signal Processing, Sensor Fusion, and Target Recognition XII*, Aug. 2003, vol. 5096, pp. 552–561, doi: 10.1117/12.484886.
[29] Zhou Wang and A. C. Bovik, “A universal image quality index,” *IEEE Signal Processing Letters*, vol. 9, no. 3, pp. 81–84, Mar. 2002, doi: 10.1109/97.995823.
[30] Y. K. Eugene and R. G. Johnston, “The ineffectiveness of the correlation coefficient for image comparisons,” *Retrieved*, pp. 1–13, 1996.
[31] A. M. Neto, A. C. Victorino, I. Fantoni, D. E. Zampieri, J. V Ferreira, and D. A. Lima, “Image processing using pearson’s correlation coefficient: Applications on autonomous robotics,” in *2013 13th International Conference on Autonomous Robot Systems*, Apr. 2013, pp. 1–6, doi: 10.1109/Robotica.2013.6623521.
[32] A. M. Neto, A. C. Victorino, I. Fantoni, and D. E. Zampieri, “Real-time dynamic power management based on pearson’s correlation coefficient,” in *15th Int. Conf. on Advanced Robotics (ICAR)*, 2011, pp. 304–309, doi: 10.1109/ICAR.2011.6088627.
[33] A. D. M. Neto, A. C. Victorino, I. Fantoni, and D. E. Zampieri, “Automatic regions-of-interest selection based on pearson’s correlation coefficient,” in *IROS Workshop on Visual Control of Mobile Robots (ViCoMoR)*, 2011, pp. 33–38.

BIOGRAPHIES OF AUTHORS

Mahmoud Rashad is a M.Sc. student at the Department of Mathematics and Computer Science, Faculty of Science, South Valley University, Egypt. He received the B.Sc. degree in computer science from South Valley University, Qena, Egypt, in 2007. He was working as software developer. Now, his research is focused on the area of information security and privacy. He can be contacted at email: nmrashad.eg@gmail.com.

Ahmed Elhadad received the B.Sc., M.Sc., and Ph.D. degrees from South Valley University, Qena, Egypt, in 2007, 2010, and 2015 respectively. He was working as an associate professor in the Computer Science Department, Faculty of Computer and Information Sciences, South Valley University, Egypt. In 2017, He worked as a Post-Doc Researcher at CRACS and INESC, Porto LA, Faculdade de Ciências, Universidade do Porto, Porto, Portugal. In 2012, he was granted mobility scholarship to (IST), Lisbon, Portugal. Now, his research is focused on the area of information security and privacy. He can be contacted at email: ahmed.elhadad@sci.svu.edu.eg.

Kamal El-Saady is currently full Professor in the department of Mathematics and Computer Science, Faculty of Science, South Valley University, Egypt. He received the Ph.D. degree in Pure Mathematics. His primary research areas are fuzzy topology and General topology. He can be contacted at email: Kehassan@sci.svu.edu.eg.